4-18-2007

Upper-Ocean Response to Hurricane Ivan in a 1/25 Degrees Nested Gulf of Mexico HYCOM

T. G. Prasad
University of Southern Mississippi, thoppil@nrlssc.navy.mil

Patrick J. Hogan
Stennis Space Center

Upper-ocean response to Hurricane Ivan in a 1/25° nested Gulf of Mexico HYCOM

T. G. Prasad[1,2] and Patrick J. Hogan[2]

Received 10 May 2006; revised 25 October 2006; accepted 16 November 2006; published 18 April 2007.

[1] A 20-layer, 1/25° nested Gulf of Mexico (GoM) Hybrid Coordinate Ocean Model (HYCOM) has been employed to examine the evolving three-dimensional ocean response to Hurricane Ivan during 14–16 September 2004. Results from several combinations of numerical experiments with and without assimilation of satellite-altimetry sea-surface height (SSH) are being analyzed and compared for the September 2004 hurricane period. A comparison of simulated zonal and meridional velocities using data assimilation shows improved agreement with profiler observations. The amplitude of the cold wake (~6°C) produced by these simulations compared reasonably well with the observed changes in SST before and after the storm; however, the region of extreme cooling varied depending on the simulated location of the warm core eddy (WCE) that had detached from the Loop Current (LC). While the simulated location of the WCE and LC in the assimilation runs agree better with satellite altimetry, the storm-induced SST cooling was 40%–50% greater than the observed cooling. Overall, ~64% of the cooling was due to vertical mixing caused by turbulence generated from strong shear-stress across the base of the mixed layer. Vertical advection (upwelling) caused a significant portion of cooling (23.4%) in those runs that included data assimilation; a three fold increase from the nonassimilative runs (7%). This enhanced upper-ocean cooling was caused primarily by the prestorm thermal stratification; a shallower thermocline (~40 m) and a stronger upper-thermocline temperature gradient compared with the nonassimilative runs. In all the experiments the air-sea exchange was a small component of the mixed-layer heat budget which overall accounted for ~4%.

Citation: Prasad, T. G., and P. J. Hogan (2007), Upper-ocean response to Hurricane Ivan in a 1/25° nested Gulf of Mexico HYCOM, *J. Geophys. Res.*, *112*, C04013, doi:10.1029/2006JC003695.

1. Introduction

[2] Warm water from the Caribbean Sea enters the Gulf of Mexico through the Yucatan Straits and then forces the Loop Current (LC). This anticyclonic rotating current with maximum flows of 1–2 m s^{-1} penetrates northward into the Gulf of Mexico and transports subtropical water with markedly different temperatures and salinities than the background Gulf of Mexico water between ocean temperatures of 18°–26°C. As the LC intrudes farther north, the instability processes associated with the LC sheds warm core eddies (WCE) having horizontal length scales of *O* (200 km [*Elliott*, 1982]) at 11–14 month intervals, which propagate westward with speeds between and 1 and 14 km d^{-1} [*Vukovich and Crissman*, 1986] over a 9–12 month period and eventually dissipate along the shelf break of Texas and Mexico.

[3] Hurricanes draw their energy from warm ocean waters. The energy input from the ocean to the hurricanes and associated intensification depends largely on the upper-ocean heat content. To quantify this, *Whitaker* [1967] first used the quantity "hurricane heat potential" which is defined as the vertically integrated heat content down to the 26°C isotherm depth [*Leipper and Volgenau*, 1972; *Goni and Trinanes*, 2003]. While all hurricanes attain their maximum intensity over warm ocean waters, there have been instances of sudden changes in intensity when passing over areas of high heat content [*Goni and Trinanes*, 2003]. In the Gulf of Mexico, maximum hurricane heat potential is found in the LC and WCE regions (~30×10^3 cal cm^{-2}), where the depth of 26°C isotherm may reach >100 m [*Leipper and Volgenau*, 1972]. These underlying preexisting oceanic mesoscale features have far more importance in the heat and moisture fluxes feeding the storm than just SST as noted in previous studies. Understanding the role of these mesoscale features in the intensification of hurricanes is an ongoing research topic. Preliminary results have shown their importance in the sudden intensification of hurricanes. *Shay et al.* [2000] noted an abrupt change in the intensity of hurricane Opal (28 September to 5 October 95) when it passed over a large WCE and *Hong et al.* [2000] studied the coupling between the WCE and Opal in an atmospheric-ocean coupled model. Hurricane Mitch occurred in the Caribbean Sea in October of 1998 and Bret in the Gulf of

[1]Department of Marine Sciences, University of Southern Mississippi, Stennis Space Center, Mississippi, USA.
[2]Naval Research Laboratory, Stennis Space Center, Mississippi, USA.

0148-0227/07/2006JC003695

Mexico in August of 1999 [*Goni and Trinanes*, 2003] and Katrina in August of 2005 [*Scharroo et al.*, 2005] also experienced very similar intensification while passing over LC and WCE regions. Two other hurricanes that may have undergone similar intensification are Ivan in September 2004 and Rita in September 2005. These examples clearly demonstrate the role of warm oceanic features in providing a positive feedback to the overlying storm by intensifying the storm.

[4] Hurricanes also cause significant SST cooling which provides negative feedback to the overlying storm by weakening the intensity of the storm. SST dropped as much as 6°C in response to the passage of Hurricane Hilda in 1964 [*Leipper*, 1967]. The lowering of SST during the passage of a hurricane depends on many factors such as mixed layer depth (vertical mixing) and thermocline depth (upwelling driven by the wind stress curl of the hurricane), exchange of air-sea heat fluxes and the storm's intensity and translation speed. Intense, slowly moving hurricanes cause the largest SST response [*Price*, 1981]. When a hurricane encounters the WCE, the SST cooling may be greatly suppressed primarily due to deep mixed-layer and thermocline depths of the WCE.

[5] Early studies of upper-ocean response to hurricanes included field observations [e.g., *Leipper*, 1967; *Brooks*, 1983; *Sanford et al.*, 1987; *Shay and Elsberry*, 1987; *Shay et al.*, 1989, 1998; *Dickey et al.*, 1998; *Jacob et al.*, 2000] and three-dimensional numerical ocean models [e.g., *Price*, 1981; *Price et al.*, 1994]. The ocean's response to hurricanes can be divided into two stages; a forced and a relaxation stage [*Price et al.*, 1994]. In the forced stage, hurricane-force winds drive the mixed-layer currents, SST cooling by vertical mixing (entrainment) and air-sea heat exchanges (mainly due to loss of latent heat flux). The barotropic response consists of a geostrophic current and an associated trough in sea surface height. The relaxation stage response following a hurricane's passage is primarily due to inertial-gravity oscillations excited by the storm. The mixed-layer velocity oscillates with a near-inertial period and hence so does the divergence and the associated upwelling and downwelling.

[6] Previous studies emphasized entrainment mixing as the dominant term in the mixed-layer heat budget [*Jacob and Shay*, 2003]. *Jacob et al.* [2000] suggested that entrainment mixing at the base of the mixed layer generally accounts for 75%–90% of the cooling based on observations while *Price*'s [1981] model results indicated that 85% of the irreversible heat flux into the mixed layer was through entrainment mixing. Only about 10%–15% of the cooling in the upper ocean is due to surface heat fluxes [*Price*, 1981] which would range between 2000 and 3000 W m^{-2}. *Jacob and Shay*'s [2003] estimate ranged from 10% to 30% in the directly forced region, with larger values in the WCE and LC regions. Horizontal advection is also found to be important in the mixed layer heat balance during and subsequent to the passage of hurricanes [*Price*, 1981; *Jacob et al.*, 2000]. This contribution is particularly significant in the eddy region, where maximum cooling due to geostrophic advection (-0.69°C d^{-1}) was as large as the surface heat flux term in the overall heat budget [*Jacob et al.*, 2000]. Also the strong currents associated with the preexisting oceanic mesoscale features (such as warm and cold core eddies) modulate the three dimensional mixed layer heat budget affecting sensible and latent heat fluxes to the atmosphere through horizontal advection.

[7] Hurricane Ivan (2–24 September 2004) first appeared on 2 September 2004 as a tropical depression and transformed into a category 3 hurricane after nearly three days. Ivan continued to strengthen as it passed over the warm waters of the Caribbean Sea and became a category 5 hurricane on 12 September 2004. During this period the atmospheric pressure dropped to a minimum value of 910 mb. Ivan entered the Gulf on 14 September 2004 and began to weaken after it passed the Loop Current region and by 16 September, had moved inland as a category 3 hurricane. The average translation speed of Ivan was 6 m s^{-1}. Waves as high as 27.7 m (91 feet) were observed when Hurricane Ivan passed directly over the outer continental shelf in the northeastern Gulf of Mexico [*Wang et al.*, 2005].

[8] The oceanic responses to hurricanes differ from one to the other in several respects making the study of the processes difficult. The oceanic response is further complicated by preexisting oceanic features such as LC and WCE that modulate the upper ocean heat, mass and momentum balance due to horizontal advection [*Jacob et al.*, 2000; *Jacob and Shay*, 2003]. A model that resolves these mesoscale features must be used to study the oceanic response to hurricanes in the GoM. Motivated by the sensitivity of the timing of the eddy-shedding (WCE) behavior in the model to changes in initial conditions which are vital for the realistic simulation of the upper-ocean response to Hurricane Ivan, we carried out several model experiments with and without data assimilation. The model is a 20-layer 1/25° (~4 km) nested Gulf of Mexico Hybrid Coordinate Ocean Model (HYCOM). Two primary objectives of this paper are (1) to assess the model's ability to reproduce the observed behavior of the oceanic responses to a hurricane with and without data assimilation and (2) to quantify the physical processes controlling the upper-ocean thermal structure during Ivan's passage by evaluating various heat-balance terms at 20 m, 50 m and 100 m depths. The paper is organized as follows: In section 2, details of model configurations, initial and boundary conditions (section 2.1), surface forcing (section 2.2), vertical mixing (section 2.3) and model experiments (section 2.4) are presented. Simulated quantities are compared with observations in section 3 followed by a qualitative description of the oceanic response to Hurricane Ivan. We quantify the upper-ocean physical processes governing the mixed-layer heat budget in section 4. Results are discussed in section 5 and summarized in section 6.

2. Model Description

[9] The nested-grid modeling system has a fine-resolution inner model embedded inside a coarser-resolution outer model. The fine-resolution nested GoM regional model extends northward from 18.1°N and westward from 77.4°W. It has a horizontal resolution of 1/25° (~4 km), twice the outer 1/12° (~8 km) North Atlantic model resolution and thus capable of resolving eddies more realistically and it enables an even higher-resolution nested coastal model to be run. There are 20 hybrid layers in the vertical which are identical to the top 20 layers in the outer

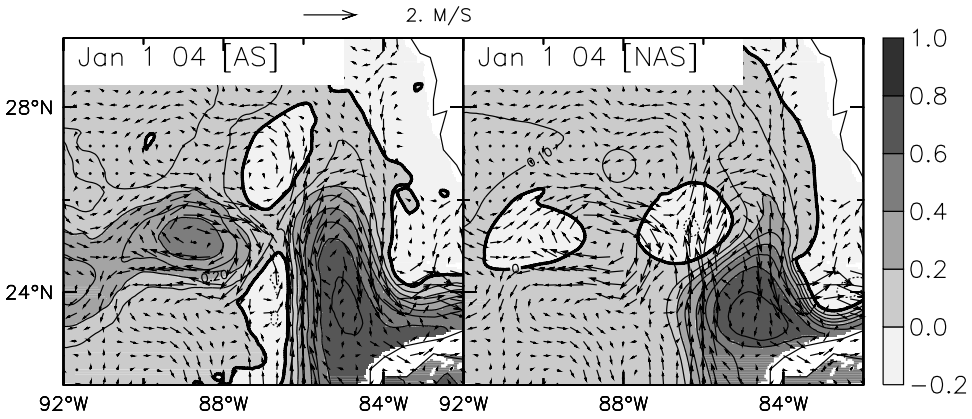

Figure 1. Comparison of model initial (1 January 2004) SSH field (m) from North Atlantic 1/12° run (left) with assimilation (AS, ATL-A) (right) nonassimilation (NAS, ATL-F). Same absolute geostrophic velocity field from satellite altimetry superimposed on both plots (cm s^{-1}) provides a comparison to observed conditions. Locations of Loop Current (LC) and WCE are different in these runs.

model. It should be noted that the bottom 5 layers of the 26 layer outer model is discarded because the densities of the deepest 5 layers in the outer model do not exist in the GoM.

2.1. Initial and Boundary Conditions

[10] The lateral boundary conditions for the GoM nested model come from the 1/12° (~8 km) North Atlantic data-assimilative HYCOM system (ATL-A). In the nested model, most of the flow enters the domain on the southern and southeastern boundaries and exits through the Florida Strait. At the open boundaries, buffer (or boundary relaxation) zones typically less than one degree wide (where the two model grids overlap) are used to relax the baroclinic model temperature, salinity, pressure and velocity components once per day towards the outer model fields (ATL-A) with an e-folding time scale of 1 to 10 days. This procedure has proven to be very robust. The method of characteristics [*Browning and Kreiss*, 1982, 1986] is used for the barotropic open boundary conditions on velocity and pressure. HYCOM currently has a robust capability for nesting with other HYCOM grids with similar vertical design. With this method all information passes from the coarse outer grid to the finer inner grid and does so offline, meaning that the nested model does not run concurrently with the outer model.

[11] The coarse-resolution outer model (ATL-A) extends from 28°S to 70°N including the Mediterranean Sea (see *Chassignet et al.* [2007] for details). The vertical resolution consists of 26 hybrid layers, with the top layer typically at its minimum thickness of 3 m. The bathymetry used in the model is derived from World Ocean Elevation data (ETOPO5) topography. The northern and southern boundaries are treated as closed, but are outfitted with 3° buffer zones in which temperature, salinity and pressure are linearly relaxed toward their seasonally varying climatological values thereby simulating the thermohaline overturning circulation. The data assimilation in the 1/12° North Atlantic HYCOM system consists of assimilating daily operational Modular Ocean Data Assimilation System (MODAS) 1/4° SSH analysis of available real-time satellite altimeter observations. The *Cooper and Haines* [1996] technique is used to project the surface information to the interior of the ocean. Relaxation to the MODAS SST analysis derived from the 5-channel Advanced Very High Resolution Radiometers (AVHRR) is also included. A similar configuration of the North Atlantic HYCOM without data assimilation (ATL-F) has been running in parallel with the assimilative system.

[12] The initial conditions for the simulations performed here are extracted from these two configurations of the North Atlantic HYCOM (ATL-A and ATL-F). All model integrations are started on January 1, 2004. Figure 1 shows the initial SSH (1 January 2004) from assimilative (ATL-A) and nonassimilative (ATL-F) Atlantic 1/12° model runs. For comparison to observed conditions, the same geostrophic velocity field from merged satellite altimetry products is superimposed on both plots. As expected, the location of WCE and the northward penetration of LC in these two model configurations are different as indicated by the SSH. The location of the WCE and LC in the assimilation run agrees with the observations while the northern edge of LC in the free run occurs farther south and there is no indication of WCE. It is these differences that subsequently lead to differences in the WCE location and SST cooling during Ivan's passage.

2.2. Surface Forcing

[13] The model is driven by fields of 10 m wind speed, vector wind stress, 2 m air temperature, 2 m atmospheric humidity, surface shortwave and long-wave heat fluxes, and precipitation. These fields are extracted from three-hourly 1° horizontal resolution Navy Operational Global Atmospheric Prediction System (NOGAPS) reanalysis product for the year 2004. Surface latent and sensible heat fluxes, along with evaporation are calculated using bulk formulae during the model run time using model SST. This has an implied restoring term, pulling the model produced SST towards the specified air-temperature thereby minimizing model SST drift.

[14] The NOGAPS wind stress is computed using the drag formulation from *Louis* [1979]. HYCOM includes several air-sea flux parameterization schemes to determine the exchange coefficients for heat fluxes. While the values of these coefficients under high winds are an ongoing

research topic [*Powell et al.*, 2003], the exchange coefficients for heat (i.e., C_L, and C_S) used here have a simple polynomial dependence on wind speed, and a linear dependence on the air-sea temperature difference (see *Kara et al.* [2002] for details). Briefly, latent heat flux (Q_L) and sensible heat flux (Q_S) are computed using the equations

$$Q_S = C_S C_p \rho_a V_a (T_a - T_S),$$

$$Q_L = C_L L \rho_a V_a (q_a - q_s),$$

$$C_L = C_{L0} + C_{L1}(T_S - T_a),\ C_S = 0.95 C_L,$$

$$C_{L0} = 10^{-3}\lfloor 0.8195 + 0.0506\hat{V}_a - 0.0009\left(\hat{V}_a\right)^2 \rfloor,$$

$$C_{L1} = 10^{-3}\lfloor -0.0154 + 0.5698\left(1/\hat{V}_a\right) - 0.6743\left(1/\hat{V}_a\right)^2 \rfloor.$$

V_a is wind speed at 10 m above sea level; T_a is air-temperature; T_S is model SST; C_p is specific heat of air (1004.5 J kg^{-1} K^{-1}); and L is latent heat of vaporization (2.5×10^6 J kg^{-1}). The air-density (kg m^{-3}) is determined using the ideal gas law; $\rho_a = 100\ P_a/\lfloor R_{gas}(T_a + 273.16)\rfloor$, where P_a is set to 1013 hPa. The mixing ratio values for air (q_a at T_a) and sea (q_s at T_s) are calculated using a simplified version of the original formulation for saturation vapour pressure (e_s) presented by *Buck* [1981].

2.3. Vertical Mixing

[15] HYCOM includes several turbulence closures to represent vertical mixing. In addition to the Kraus-Turner model used in MICOM and modified to run with hybrid coordinates, HYCOM has been equipped with the Price-Weller-Pinkel dynamical instability model (PWP [*Price et al.*, 1986]), the K-Profile Parameterization (KPP [*Large et al.*, 1994, 1997]), the Mellor-Yamada level 2.5 (MY [*Mellor and Yamada*, 1982]) and the NASA Goddard Institute for Space Studies level 2 (GISS [*Canuto et al.*, 2001, 2002]). An evaluation of these vertical mixing schemes in the HYCOM in low-resolution climatological simulations of the Atlantic Ocean is discussed by *Halliwell* [2004]. Technical details of the implementation of these vertical mixing schemes have been included in the HYCOM User's Manual [*Bleck et al.*, 2002]. The experiments reported here included the GISS mixing scheme. This vertical mixing model was constructed using the Reynolds stress model (see *Canuto et al.* [2001, 2002, 2004] for details). The GISS model included a more physical representation of several aspects of the Reynolds stress model, in particular a better representation of the velocity and temperature pressure correlations.

[16] The simulation of mixed layer deepening and cooling during the storm's passage strongly depends on the choice of a vertical mixing scheme. Recent studies of upper-ocean responses to Hurricane Gilbert based on several bulk mixed layer entrainment schemes revealed significant differences in the heat and mass budgets [*Jacob et al.*, 2000; *Jacob and Shay*, 2003]. Though most schemes differ in their physical basis, direct comparisons indicate no clear advantage between several schemes. While these discrepancies among the schemes make it hard to justify the suitability of a particular scheme, GISS has a number of advantages over other schemes including (1) the higher predictability of the turbulent mixing $R_i \approx O(1)$ compared to MY-type models which cut off mixing too early leading to shallow mixed layers [*Martin*, 1985] (2) the number of adjustable parameters is one (compared to 11 in KPP) and (3) the latitudinal dependence of the diffusivities in the thermocline (which KPP does not account for). Thus KPP is basically a diagnostic model whereas GISS is prognostic and thus much more suitable for climate studies. The primary conclusions drawn here using GISS also stand valid for other vertical mixing schemes.

2.4. Model Experiments

[17] The major mesoscale features of oceanic circulation in the GoM are the LC and WCE that detach from it. During its passage, Hurricane Ivan encountered both of these predominantly anticyclonic circulation features. Therefore, realistic prestorm conditions including the major currents and eddies prior to the passage of Ivan, are vital for the accurate simulation of the upper-ocean response. This is achieved here by performing a series of model experiments using a nested GoM regional model. For simplicity, our control (main) run does not include data assimilation. The initial condition for this control run comes from a non-assimilative version of 1/12° North Atlantic system (ATL-F) and the simulation does not include data assimilation (free run). As we shall see in the following sections, the control run failed to simulate the WCE location consistent with the observations during the Hurricane Ivan period. To resolve this issue, we design four additional experiments by (1) changing the initial conditions and (2) including the data assimilation during the model run. In the first experiment, we initialize the control run with more realistic initial conditions from an assimilation version of 1/12° North Atlantic model (ATL-A). The second experiment is an exact repeat of the control run except that the simulation included data assimilation throughout the period. Comparison of this experiment with the control run will determine the impact of the assimilation. We devise a scheme to identify these experiments by taking into account two aspects of the simulation (1) initial conditions and (2) run-time specifications. On the basis of the model's initial condition (e.g. assimilation, free-run) and run-time specifications (e.g. assimilation, free-run), we denote these simulations FF (control run), AF (experiment 1) and FA (experiment 2) respectively (e.g. in AF, A stands for assimilation, the initial condition, and F stands for free-run, also nonassimilation, the run-time specification). An exact repeat of AF but with data assimilation (AA) produced identical results with that of FA and therefore is not presented here.

[18] Two additional experiments that are variants of these three runs are also performed to address specific questions on the effectiveness of the nonassimilative versus assimilative runs. The first experiment is an exact repeat of the control run except that the assimilation is applied only through 1–30 September 2004 (FF-A9). FF-A9 differs from FA in that assimilation is applied from 1-January to 31-December 2004. In the second experiment, the control run is repeated with data assimilation except during the period 1–30 September 2004 (FA-F9). These two simulations are carried out only for the period 1–30 September

Table 1. Model Experiments

Experiments	I.C.[a]	I.C. Time	I.C. Experiments	Run	Period
FF	NAS[b]	1-Jan 04	ATL-F	NAS	Jan-Dec
AF	AS[c]	1-Jan 04	ATL-A	NAS	Jan-Dec
FA	NAS	1-Jan 04	ATL-F	AS	Jan-Dec
FF-A9	NAS	1-Sep 04	FF	AS	1-30 Sep
FA-F9	AS	1-Sep 04	FA	NAS	1-30 Sep

[a]I.C., initial conditions.
[b]NAS, nonassimilation.
[c]AS, assimilation.

2004 by taking initial conditions (1-September 2004) from the experiments FF and FA, respectively. Thus, in FF-A9, FF denotes the baseline run from which initial conditions are taken and A9 indicates the run-time specifications (assimilation during 1–30 September 2004). The initial conditions (1-September 2004) for FA-F9, like AF, includes the correct location and structure of the WCE and LC. These model experiments are summarized in Table 1. It should be noted that in all the experiments reported here, SST evolves as a result of physical processes without relaxing it to MODAS SST. This enables us to compare the mixed layer heat-budget with and without data assimilation. The data from these experiments analyzed during the Ivan period (September, 2004) are presented in the following sections.

3. Results

[19] Results from three model experiments are presented. The impact of data assimilation on the model simulations are assessed by comparing SSH, SST and velocity fields from FF and FA with observations. The SSH variance (m^2) from FF and FA is compared with that derived from altimetry for the year 2004 in Figure 2. Daily SSH is used. The energy level of the WCE is realistic and the eddy detachment from the LC occurs at approximately the correct latitude. The location of extreme variance coincides with the WCE and its westward propagation. The amplitude is larger (smaller) in the simulation without (with) data assimilation.

[20] Time series of SST from National Data Buoy Centre (NDBC) buoy 42001 located on the left side of Ivan's track (89.66°W, 25.84°N) is compared with model SST (Figure 3a). The inset plot is for the September time-period; the focus of the study. It should be noted that the model SSTs are the mixed layer temperature, while the buoy measures the actual surface temperature. Simulated SSTs between May and August 2004 are in good agreement with the buoy SSTs while they depart systematically during the poststorm period. In September the buoy SST indicated two periods of cooling; the first event took place during the storm and the second major cooling occurred after Ivan made landfall. The cooling during the storm was primarily due to the net surface heat loss from the ocean ($\sim$300 W m^{-2}) and wind-driven turbulent mixing due to strong wind (16 m s^{-1}, figures not shown). The cooling during the poststorm period was not driven by surface heat flux, but was most likely due to advection or upwelling.

[21] Mixed-layer zonal and meridional velocity components from FF and FA are compared with the altimetry derived absolute geostrophic velocity vectors. Mindful that the model velocity fields include a wind-driven component, the one-to-one comparison should be interpreted carefully. The area averaged (88°–86°W, 24°–26°N) velocity fields are shown in Figures 3b and 3c. The velocity components from FA agree favorably with the altimetry, but they differ significantly with FF. The large differences in the velocity components that occurred during April–August are associated with the differences in the location of the WCE among the two model runs which is reflected in SSH (Figure 3d). The separation of WCE from the LC in FF took place in April (indicated by peak SSH) whereas that in FA occurred in August consistent with observations. As we shall discuss in the following sections, the different time of separation of WCE from the LC in these runs led to changes in the advective heat transport during the passage of Ivan.

[22] Ivan passed directly over an array of 14 Acoustic Doppler Current Profilers (ADCPs) deployed along the outer continental shelf and upper slope in the northeastern Gulf of Mexico as part of the Slope to Shelf Energetics and Exchange Dynamics (SEED) project [*Wang et al.*, 2005] (W. J. Teague et al., Observed oceanic response over the upper continental slope and outer shelf during Hurricane Ivan, submitted to *Journal of Physical Oceanography*, 2006, hereinafter referred to as Teague et al., submitted manuscript, 2006). Simulated current profiles were compared with ADCP measured zonal (U, m s^{-1}) and meridional (V, m s^{-1}) ocean currents from moorings M3 and M13 situated to the right of Ivan's track to evaluate the model's skill in predicting the ocean response. The choice of these moorings for comparison was made according to their locations; M3 being located in the outer shelf (87.84°W, 29.47°N) at a depth of $\sim$60 m and M13 being located along the continental slope (87.83°W, 29.16°N) at a depth of 1000 m, thereby enabling us to compare the ocean's response to Ivan across the shelf break. M3 (M13) recorded current profiles with 2 m (10 m) vertical resolution every 15 (60) minutes with an accuracy of 0.5% ± 0.5 cm s^{-1} ($\sim$1 cm s^{-1}). A 24 hour Parzen window smoothing has been applied on these data for direct comparison with model fields. A detailed, nonsmoothed, version of the velocity components from all 14 moorings are plotted and discussed by Teague et al. (submitted manuscript, 2006).

[23] Time series of zonal and meridional velocity components from moorings M3 and M13 in the upper 50 and 500 m, respectively, and the corresponding fields from model simulations FF and FA are depicted in Figure 4. Overall, simulated currents compared well with the observations and zonal component dominated the flow in part due to the flow being parallel to the isobaths. In the outer shelf (M3), the zonal flow during the prestorm period (5–12 September) was eastward with peak velocities of 0.5 m s^{-1} at 20–30 m. Both simulations reproduced this flow with assimilation run FA being the closest match. The storm-induced flow reversal in the upper 50 m was evident in both the observations and simulations with maximum velocities exceeding 1 m s^{-1}. The subsurface intensified eastward flow (0.4 m s^{-1}) at M3 seen after 25 September was less pronounced in the model (0.2 m s^{-1}). In the wake of the storm, the zonal velocity oscillated with alternating eastward and westward motion indicating near-inertial

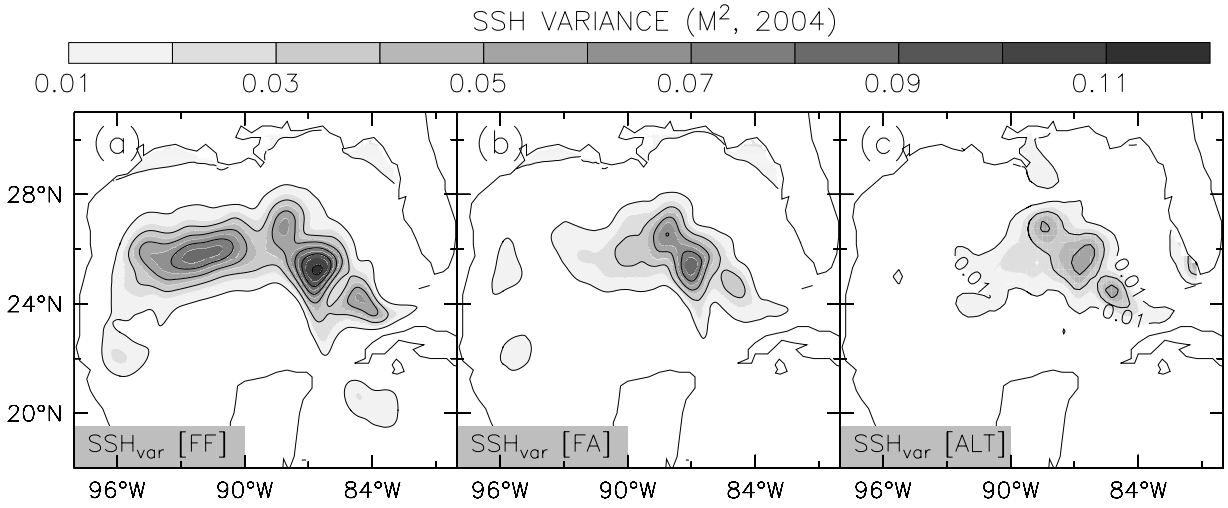

Figure 2. SSH variance from model experiments (a) FF, (b) FA, and (c) altimeter data. Contour interval is 0.01 m^2.

currents which the model successfully simulated. Though much weaker than *U*, the simulated meridional velocity agreed reasonably well with ADCP with one major exception; a strong southward flow (0.3 m s^{-1}) seen in ADCP data between 17 and 21 September was absent in the model.

[24] The upper-ocean currents response to Ivan at M13 was not significantly different from that at M3. The storm-forced maximum simulated zonal velocities in FF slightly underestimated (0.3 m s^{-1}) the observed maximum of 0.5 m s^{-1} below ~200 m, but agreed better in FA. Prestorm and poststorm velocities were also greatly improved when simulation included the data assimilation. For example, the magnitude of the prestorm eastward flow in FF was 30%–40% larger than the ADCP data, but agreed better with FA. The agreement between the observed and modeled meridional velocities was reasonably good. A similar degree of agreement has also been evident for all 12 other mooring locations which are not discussed here.

[25] Time series of zonal and meridional wind stresses from NOGAPS are shown in Figure 5a. A maximum wind stress of 1.82 N m^{-2} was attained during the passage of Ivan. The time series of mixed layer temperature (SST), thickness (MLD), salinity (SSS), and surface heat flux (SHF) averaged for the region 88°–86°W, 24°–26°N from these three experiments are shown in Figures 5b–5e and Tropical Microwave/Imager (TMI) derived SST for comparison in Figure 5b. In general, the SST cooling during the storm was in reasonable agreement with the observations. The prestorm MLD of a ~10 m increased to ~45 m during the storm and the corresponding SSTs or mixed layer temperature decreased from ~28.5° to ~25°C (~3.5°C decrease) except in the run that included assimilation. The cooling simulated by FF was in better agreement with the TMI. Despite a shallower ML (~30 m), the SST cooling in FA was far more intense (~22.5°C) than the other two experiments and TMI. It is likely that part of the increase in the MLD is offset by the upwelling which reduced the mixed layer thickness by 15 m (discussed further in section 4). *Greatbatch* [1985] noted the role played by the upwelling of water and the associated reduction in mixed-layer depth in lowering SST during the passage of a storm. Poststorm model SSTs were cooler by ~2°–4°C than TMI. These SST differences among the simulations were reflected in the net surface heat flux through surface latent and sensible heat fluxes terms, which were calculated using the model SST. The net surface heat flux showed a loss of ~150 W m^{-2} to the atmosphere during the storm which partly accounted for SST cooling in AF and FF, but it was only about 50 W m^{-2} in FA. As expected, this large heat loss was primarily due to the high latent heat flux exchange caused by the high winds. Poststorm MLD in all experiments dramatically dropped to ~5 m with SSTs steadily increasing. The poststorm warming was in part a result of weaker winds along with cool SSTs which reduced the latent heat loss significantly leading to 150 W m^{-2} heat flux gain by the ocean. What is important here is that surface heat loss to the atmosphere was not a significant contributor to SST cooling during the storm.

[26] Consistent with SST changes, SSS also showed significant differences among the three experiments though freshwater fluxes (evaporation – precipitation) from these experiments were nearly the same. The maximum surface freshening occurred in FA where it dropped to 35.6 psu from prestorm value of 35.8 psu. The lowest SSS associated with the storm occurred one day later than the SST minimum. In the Gulf of Mexico, low salinity waters are located below ~100 m (except in the northern Gulf) with salinity increasing with depth in the upper 100 m. If this surface freshening occurs as a result of upwelling, then it has to come from much deeper depths. On the other hand, upwelling or mixing of cooler water from a relatively shallow thermocline yielded instant SST cooling.

[27] The complex nature of interactions between the WCE and Hurricane Ivan are evident in Figure 6. TMI derived SST (shaded) superimposed with altimeter SSH (contours) before (10 September 2004) and after (16 September 2004) the passage of Hurricane Ivan (SSTs are three day averages ending on 10 and 16 September 2004, respectively) and the corresponding model-derived SST (snapshot) and SSH from the three experiments are displayed in Figure 6.

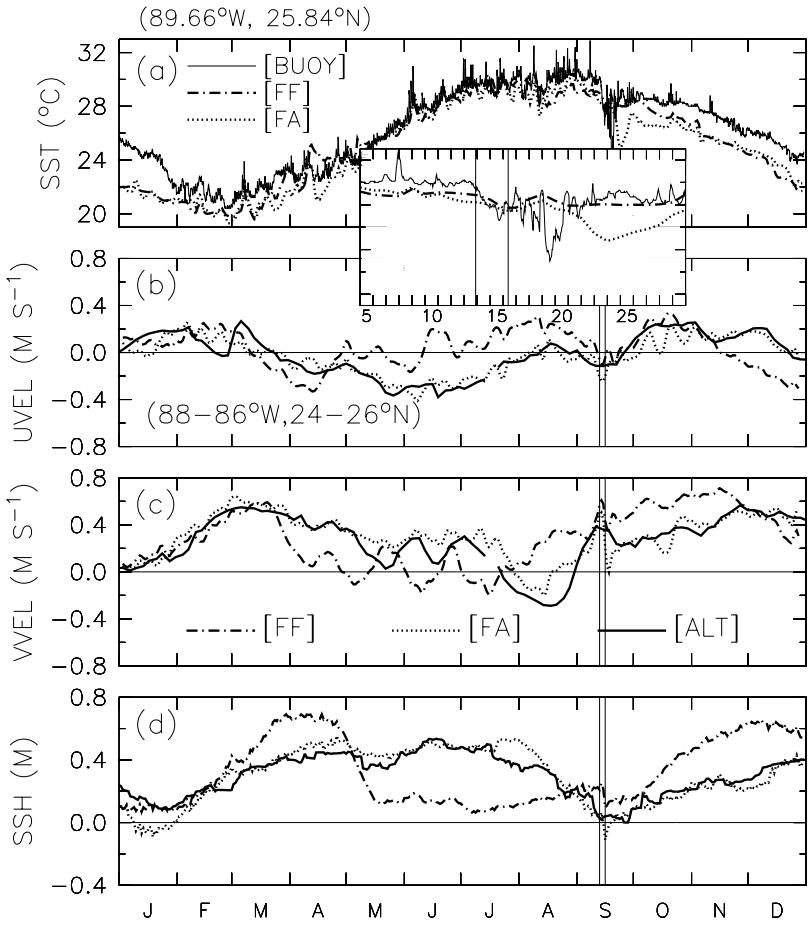

Figure 3. Simulated SSTs from FF (without assimilation) and FA (with assimilation) is compared with a National Data Buoy Centre (NDBC) buoy (42001) at 89.66°W, 25.84°N located to the west of Ivan's track. The inset plot is for September time frame; the focus of the study. Comparison of model (b) zonal and (c) meridional velocity components (m s^{-1}) with observed absolute geostrophic velocities (altimetry) and (d) SSH (m). These fields are averaged over the 2° × 2° box (88°–86°W, 24°–26°N) shown in Figure 6. A five-day smoothing has been applied to daily model fields to make them consistent with five-day altimetry data. The vertical lines in each plot indicate the time of arrival and landfall of Ivan in the Gulf of Mexico.

The right panel of Figure 6 shows the corresponding SST differences (ΔSST). Prestorm SST (10 September 2004) in the Gulf was >30°C almost everywhere resulting from the intense summer solar heating except a small region southwest of the Florida coast (remnants of cooling from Hurricane Frances about two weeks earlier). The altimeter SSH revealed the existence of a cyclonic cold-core eddy (CCE, ∼87°W, 25°N) and an anticyclonic WCE (∼89.2°W, 26.7°N) along Ivan's track. Prestorm SST, however, did not indicate the presence of these mesoscale eddies. What is interesting here is that the amplitude of SST cooling in the wake of the hurricane was not continuous. The maximum (minimum) cooling occurred outside (inside) the WCE and LC regions suggesting that the upper-ocean cooling was directly influenced by these preexisting mesoscale features. In contrast to the well-documented rightward bias of the SST cooling response to most hurricanes, the maximum SST cooling occurred to the left of the Ivan's track, especially west of the LC region (TMI SST during September 16). *Leipper*'s [1967] observations of the SST response to Hurricane Hilda did not show a rightward bias (see their Figure 8).

[28] Though hurricane-induced SST cooling was certainly evident in all three experiments, the details of the cooling especially the location of maximum cooling differed from the TMI and among these three simulations. These differences were caused primarily by the differences in the location of warm and cold core eddies which are clear from the superimposed SSH fields. While LC and WCE in AF and FA were located in the vicinity of the observed location, the LC in FF penetrated farther north and WCE was situated ∼395.7 km farther southwest (92.2°W, 26.1°N) than altimetry (88.3°W, 26.8°N). The CCE in FF was located slightly (∼78 km) farther northwest (87.5°W, 25.5°N) than altimetry (87.1°W, 24.9°N). Consequently, the region of maximum cooling occurred farther north of the observed minimum. Coincident with the southward shift of the WCE, the maximum SST cooling in AF occurred farther south compared with TMI. The location of the greatest cooling in FA agreed with the TMI observations, but the amplitude of simulated SST differences (ΔSST) induced by

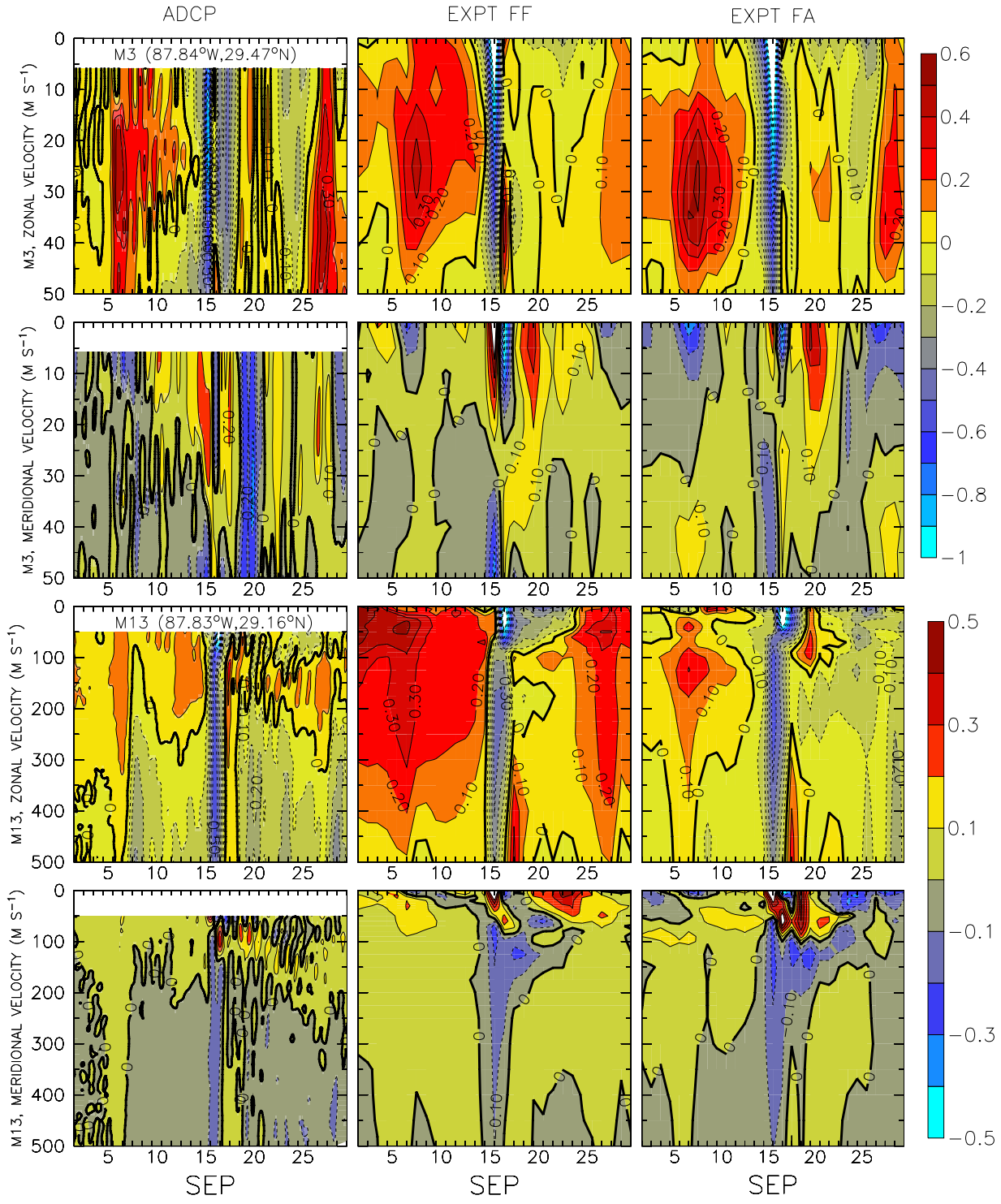

Figure 4. Time series of observed zonal (U) and meridional (V) velocity components from moorings M3 (87.84°W, 29.47°N) and M13 (87.83°W, 29.16°N) in the upper 50 and 500 m, respectively, and the corresponding fields from model simulations FF and FA. A 24-hour Parzen window smoothing has been applied on these mooring data. Contour interval is 0.1 m s^{-1}. These moorings are located to the right of Ivan's track. Daily model fields are used. Note different color scaling is used for U and V. Positive U (V) indicates eastward (northward) flow.

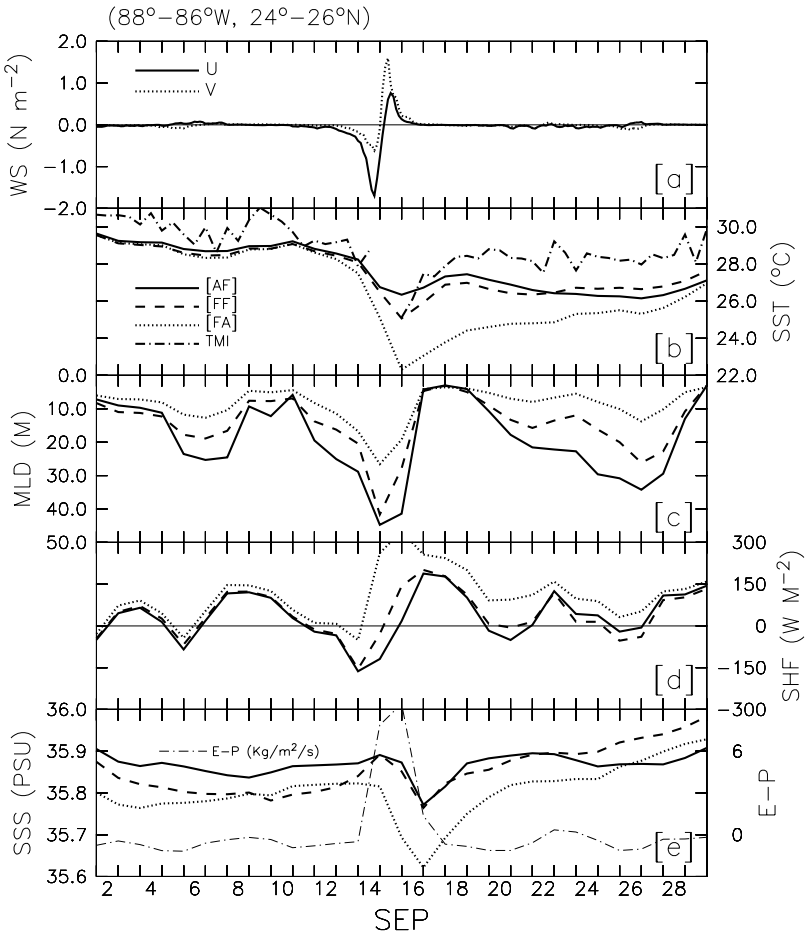

Figure 5. Time series of (a) zonal (east-west) and meridional (north-south) wind stress (N m^{-2}), model (b) mixed layer temperature (SST, °C), (c) mixed layer depth (MLD, m), (d) surface heat flux (SHF, W m^{-2}), and (e) mixed layer salinity (SSS, psu) from AF, FF and FA. Also included in Figure 5b is the TMI derived SST, and model evaporation-precipitation (E-P, kg m^{-2} s^{-1}) is included in Figure 5e.

Ivan was as high as 10°C and was spread over a much larger area.

[29] In contrast to TMI, the signature of the LC and WCE were clearly identifiable in the prestorm SST maps in all experiments. Simulated prestorm SSTs (especially northwest of LC) were generally colder than those derived from the TMI by ~1°C. The coincidence of the extreme cooling within the cyclonic eddy in all experiments during Ivan's passage suggests that upwelling was likely an important mechanism for upper-ocean cooling. The poststorm SSH dropped from the prestorm conditions by ~10 cm due to shoaling of upper thermocline driven by the curl of the wind stress. While the amplitude of simulated SST differences were within the observed limits (except for FA), there were significant differences between the simulated and observed location of maximum cooling. What is however interesting in both simulated and observed cooling is that the cooling was only about 1°–2°C within WCE and LC regions. These results suggested a clear modulation of upper-ocean cooling by the WCE and LC systems.

[30] The background circulation associated with these systems combined with directly forced wind-driven currents during the passage of the storm also played an important role in the modulation of SST cooling via horizontal advection. To demonstrate this, we show prestorm (10 September) and storm (15 September) ocean surface currents from AF, FF and FA in Figure 7. Prestorm surface circulation in the Gulf was largely geostrophic; the magnitude of the LC (~1 m s^{-1}) is comparable with the absolute geostrophic velocity vectors derived from the satellite altimetry (Figure 1). Because of the westward displaced WCE in FF, the LC penetrated farther north than in the other two experiments. During the storm, directly forced wind-driven currents dominated the surface circulation in all experiments and the structure of the LC was not discernable. However, the effect of prestorm circulation associated with the WCE and LC on the storm induced currents was evident. For example, the westward flowing current to the southern flank of the WCE in AF was slightly stronger than that in FF. The strongest currents exceeding 2 m s^{-1} were found to the right of Ivan's track, consistent with the most intense winds associated with the eye-wall being located in the northeast quadrant of the hurricane, leading to large current shear across the mixed layer. To the left of the track the currents were somewhat weaker. This suggests that the horizontal

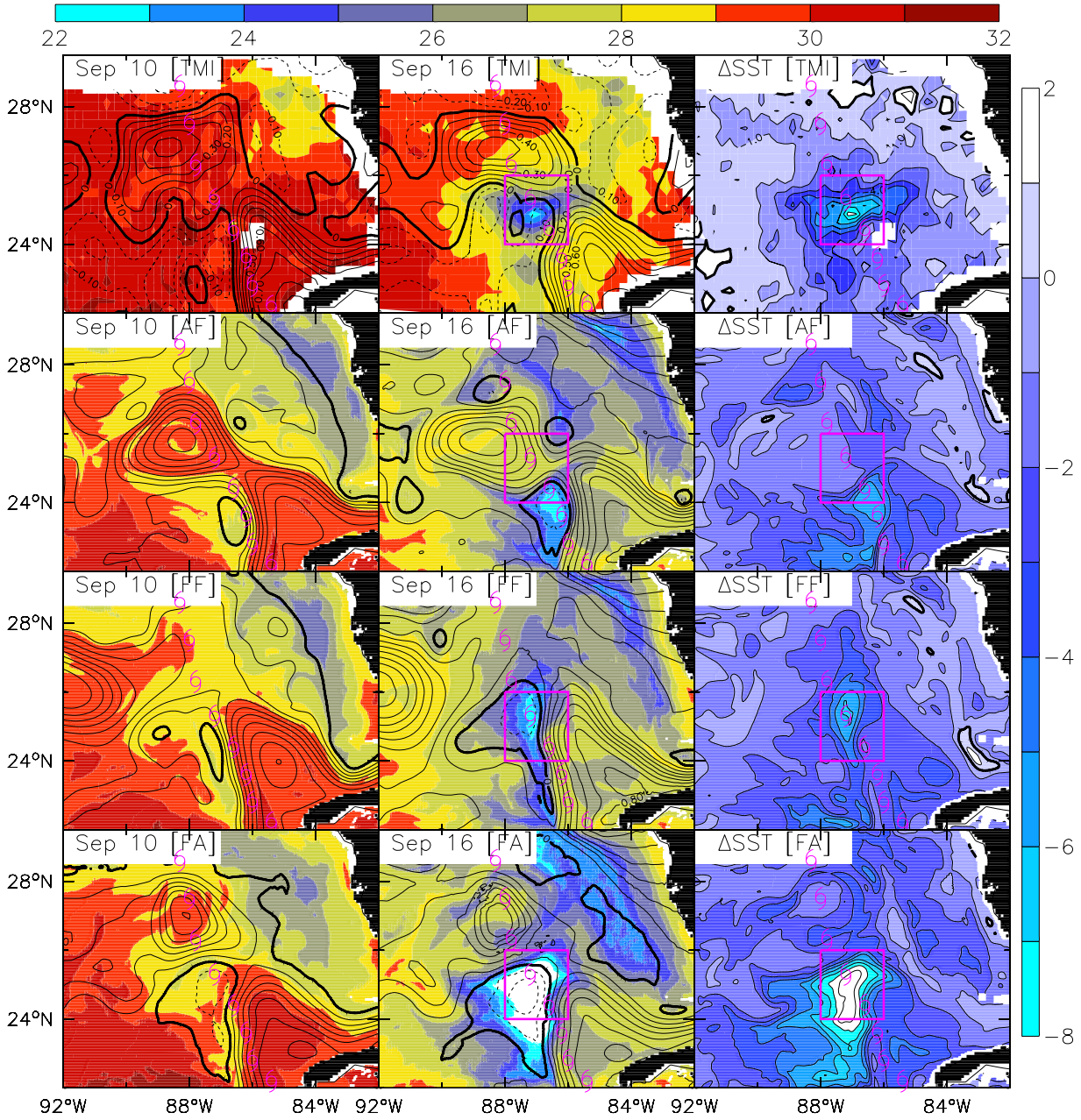

Figure 6. Prestorm (10 September) and poststorm (16 September) SSTs and the corresponding prestorm and poststorm SST differences, ΔSST (shaded, °C) from the Tropical Microwave/Imager (TMI) and from model experiments AF FF and FA arranged from top to bottom panels, respectively. Prestorm and poststorm sea surface height (SSH, m) from altimetry and models are superposed on these plots as contours. TMI SSTs are three-day averages ending September 10 and 16, respectively. Contour interval for SST is 1°C, SSH is 0.1 m and ΔSST is 1°C. The storm track of Hurricane Ivan compiled by the National Hurricane Center is plotted for every 6-hour interval. The solid box (2° × 2°, 88°–86°W, 24°–26°N) represents the area of interest for the analyses presented here. Ivan passed over this region on 15 September 2004. Altimeter indicates a warm core eddy (WCE) near 89.2°W, 26.7°N and a smaller cold core eddy (CCE) near 87.1°W, 24.9°N, southeast of the larger WCE.

advection by wind-driven currents was an important mechanism for the mixed-layer heat balance.

[31] While SST cooling varied by nearly ~0.5°C between AF and FF, there were significant differences between FA and FF. The larger simulated SST cooling in FA were not a result of enhanced shear-induced vertical mixing because storm induced currents in all cases were nearly the same (Figure 7). The different response of the SST in the three experiments (AF, FF and FA) can be explained in part by differences in the prestorm thermal stratification. A shallower (deeper) thermocline is likely to produce stronger (weaker) upper-ocean cooling with a given surface wind force. The depth of 20°C isotherm (D_{20}, measure of thermocline depth) prior to the passage of Ivan indicated a

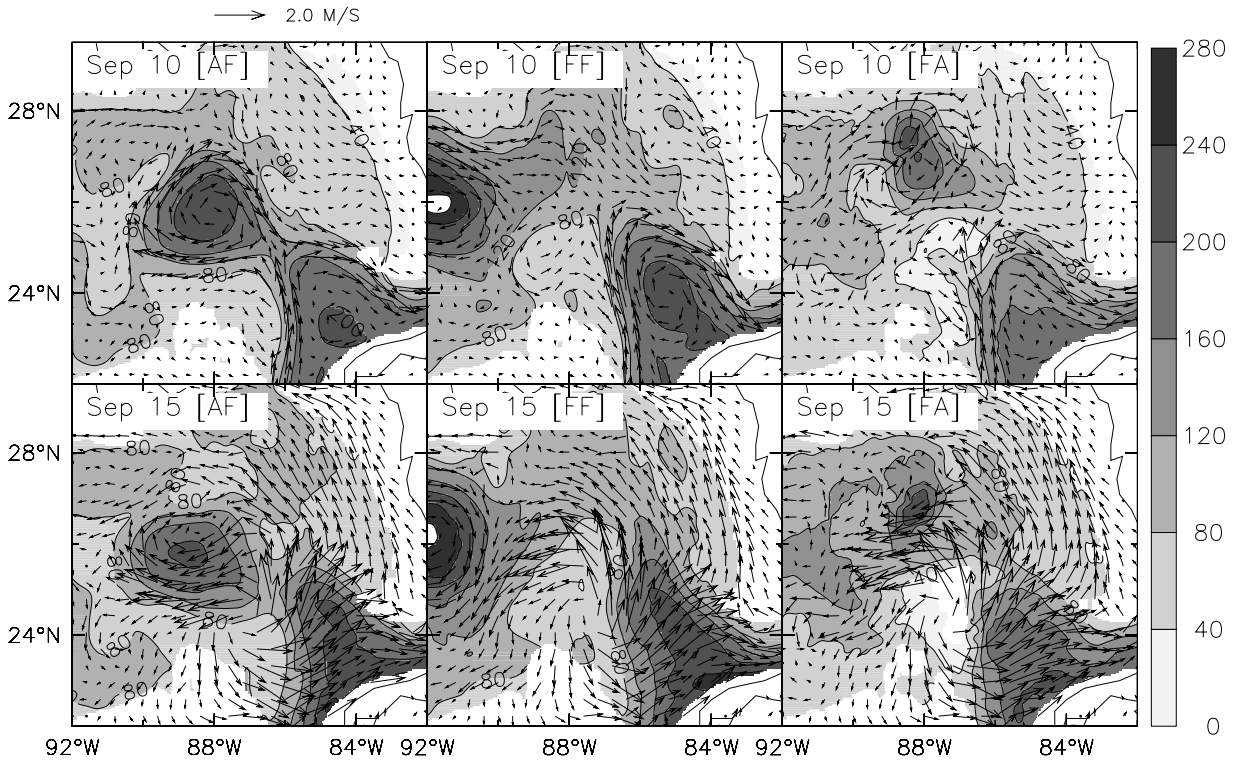

Figure 7. Comparison of ocean surface currents (m s^{-1}) before (10 September, top) and during (15 September, bottom) the storm from (left) AF, (middle) FF and (right) FA, respectively. Shaded regions indicate the corresponding depth of 20°C isotherm (D_{20}, m) except poststorm (16 September, bottom) D_{20} is shown.

shallow thermocline west of ~87°W in all experiments (Figure 7). The prestorm (September 10) values of D_{20} in AF and FF remained similar (~80 m), while there was a significantly shallower D_{20} by 40 m in FA. It is these differences in D_{20} that lead to different SST responses during the passage of Ivan. Thus, the wind-driven mixing associated with the storm produced a greater cooling in FA where the prestorm thermocline was shallower. The physical processes leading to different SST responses in these experiments are quantified in the following sections.

4. Mixed Layer Heat Budget

[32] What were the physical processes affecting upper-ocean cooling during Ivan's passage? To address this, we calculate the mixed layer heat-budget terms from these runs and will present them in the following sections and summarize them in Table 2. The mixed-layer processes being discussed here were taken at a constant depth of 20 m (slab = 20 m) rather than time varying MLD. The heat-budget terms are also presented below the mixed-layer for two depths (50 and 100 m) to determine the underlying processes leading to subsurface temperature changes. These terms are averaged over the area between 88°W and 86°W and 24°N and 26°N (2° × 2° box, Figure 6) where the maximum upper-ocean cooling occurred. The heat-budget terms can be written as $Q_T = -Q_{U+V} - Q_W + Q_S + Q_{DV} + Q_{DH}$; that is, the rate of change of heat storage (Q_T) is the sum of horizontal (Q_{U+V}), vertical (Q_W) advection, surface heat flux (Q_S), vertical (Q_{DV}) and horizontal diffusion

Table 2. Prestorm (14 September), Storm (15 September) and Poststorm (16 September) Heat-Budget Terms From Various Model Experiments and Percentage Contribution of Each Term in Parentheses[a]

	14 Sep			15 Sep					16 Sep		
Experiments	AF	FF	FA	AF	FF	FA	FF-A9	FA-F9	AF	FF	FA
Q_T	−325	−152	157	−2055	−1421	−2870	−2839	−1824	−306	305	2061
Q_S	−177	−168	−65	−124	−34	256	366	59	11	137	334
	(54.4)	(110.5)	(−41.2)	(6.1)	(2.4)	(−8.9)	(−12.9)	(−3.2)	(−3.7)	(44.8)	(16.2)
Q_{DV}	−82	−95	−165	−896	−1045	−2002	−2095	−1079	−150	−250	−259
	(25.0)	(62.8)	(−104.9)	(43.6)	(73.6)	(69.8)	(73.8)	(59.2)	(48.9)	(−81.8)	(−12.6)
Q_{U+V}	−47	94	204	−964	−229	−460	−443	−629	−178	235	1846
	(15.0)	(−62.1)	(129.9)	(47.0)	(16.1)	(16.0)	(15.6)	(34.5)	(58.0)	(77.0)	(89.6)
Q_W	−20	16	181	−72	−114	−666	−669	−176	11	183	140
	(6.2)	(−10.8)	(115.4)	(3.5)	(8.0)	(23.2)	(23.6)	(9.6)	(−3.5)	(59.8)	(6.8)

[a]Heat-budget terms from experiments FF-A9 and FA-F9 are included only for 15 September. Unit is W m^{-2}. These are daily snapshots averaged for the 2° × 2° box described in the text.

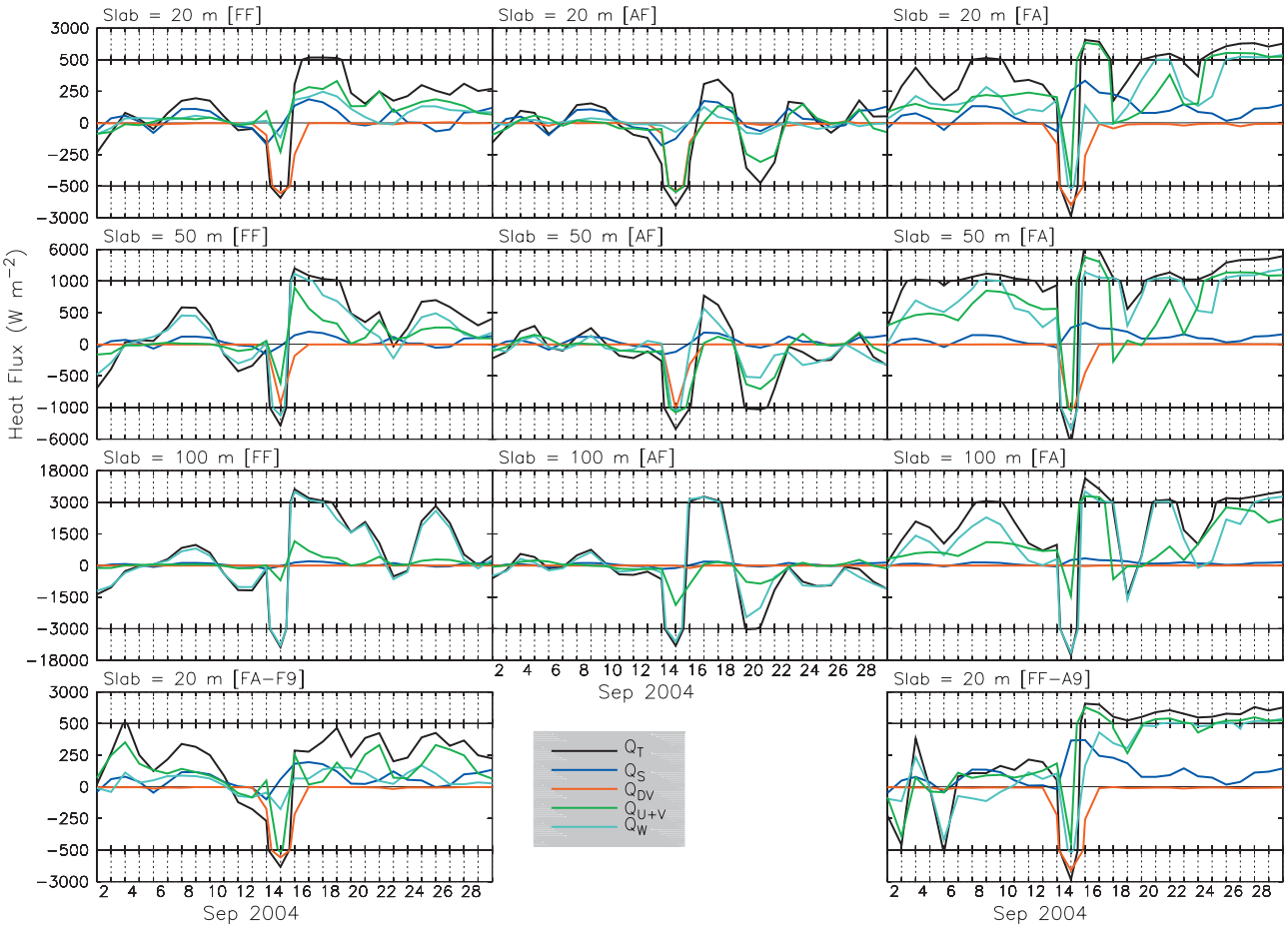

Figure 8. Area-averaged (88°−86°W, 24°−26°N) heat-budget terms in W m^{-2} at three depths 20 m, 50 m and 100 m from FF (left, top three panels), AF (middle panels), FA (right, top three panels) and heat-budget terms at 20 m from FF-F9 (left, last row) and FA-F9 (right, last row) during September 2004. The heat-balance terms include rate of change of heat storage (Q_T), surface heat flux (Q_S), vertical diffusion (Q_{DV}), horizontal diffusion (Q_{DH}) horizontal advection (Q_{U+V}) and vertical advection (Q_W); $Q_T = -Q_{U+V} - Q_W + Q_{DV} + Q_{DH} + Q_S$. Since horizontal diffusion (Q_{DH}) is negligibly small, it is not plotted. These are daily snapshots. Note that for clarity y-axis has different divisional lengths.

(Q_{DH}) terms. Since horizontal diffusion (Q_{DH}) is negligibly small it is not plotted. The time series of heat-budget terms at three depths 20 m, 50 m and 100 m which are representatives of the mixed layer, mixed layer base and upper-thermocline, respectively, from FF, AF, and FA are displayed in Figure 8. These are model daily snapshots.

4.1. Control Run FF (Nonassimilation)

[33] Overall, prestorm SST changes were caused primarily by the surface heat flux term (Q_S) while horizontal advection (Q_{U+V}) contributed to the poststorm net warming. Vertical diffusion (Q_{DV}, wind-driven mixing) dominated (−1045 W m^{-2}, 74%) the net upper-ocean cooling (−1421 W m^{-2}) during the passage of Ivan and horizontal advection caused a loss of 228.5 W m^{-2} (16%) of heat from the ocean. Following the passage of Ivan on September 16, the upper-ocean started warming at a rate 304 W m^{-2} due to the combined effects of surface heat flux and advection terms (Q_{U+V+W}) which overwhelmed the net cooling (−250 W m^{-2}) due to vertical mixing. For the next three days the ocean gained an average 664 W m^{-2} of heat through surface heat flux (149 W m^{-2}) horizontal advection (294 W m^{-2}) and vertical advection (Q_W, 221 W m^{-2}). Thereafter, the upper-ocean continued to warm at ~225 W m^{-2}. An important result consistent with earlier studies is that the vertical mixing dominated the mixed-layer heat-balance during the storm.

[34] A major difference in heat balance terms at 50 m depth from the surface (20 m) was the role played by vertical advection in warming or cooling at the mixed-layer base. Throughout the period the rate of heat-storage (Q_T) was in general caused by vertical advection. During the storm, upwelling of colder water from below (vertical advection) was responsible for ~59% of cooling (−2262 W m^{-2}) while wind-driven vertical mixing accounted for ~23% of cooling. Both advective terms contributed to the net warming after the passage of Ivan. Vertical advection (>90%) controlled the temperature changes at 100 m. The large amplitude temperature changes that occurred below the mixed layer (50 and 100 m) during the poststorm period were a result of the inertial oscillations with a period near 28 hours, generated by the onset of hurricane-force winds (not shown). Shear-

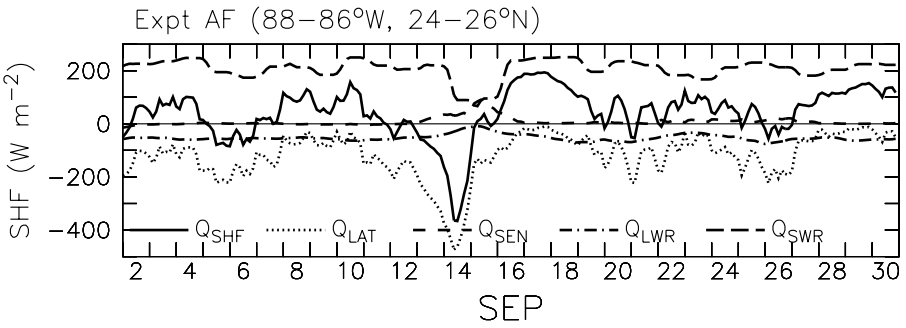

Figure 9. Box averaged three-hourly snapshots of model net surface heat flux (Q_{SHF}), latent heat flux (Q_{LAT}), sensible heat flux (Q_{SEN}), long-wave radiation (Q_{LWR}) and shortwave radiation (Q_{SWR}) in W m^{-2} from AF.

induced entrainment mixing forced by near-inertial motions after the passage of Gilbert was also noted by *Jacob et al.* [2000].

4.2. Experiment AF (Assimilation Initial Condition)

[35] A major difference between FF and AF was the location of WCE (Figures 6 and 7) which eventually altered the location of maximum cooling in AF. Thus a comparison of heat-balance terms between AF and FF delineate the influence of the WCE on SST cooling. As is evident in Figure 8, the strong ocean currents associated with the WCE in AF clearly contributed to the mixed-layer heat budget. The prestorm heat-storage rate agreed reasonably well with FF. The upper-ocean began to cool on September 11 due to the combined effects of surface heat loss from the ocean (Q_S) and horizontal advection (Q_{U+V}). About 54% of the total heat loss on September 14 resulted from the air-sea heat flux and vertical mixing accounted for 25%. As expected, this high surface heat loss was primarily due to the high latent heat flux loss (-473 W m^{-2}) caused by strong winds (Figure 9). The upper ocean cooled at a rate -2055 W m^{-2} during the storm; vertical diffusion (turbulent wind-driven mixing) contributed 44% of total heat loss and horizontal divergence (cooling) accounted for 47%. Sensible heat flux during the storm period showed a heat gain by the ocean (90 W m^{-2}) due to warmer air-temperature. Heat loss due to longwave radiation was only 10–20 W m^{-2}. A significant part of the warming that occurred following the passage of Ivan resulted from net surface heat gain by the ocean. The net-heat gain by the ocean during this period was primarily due to a reduction in latent heat flux by weaker winds and cool SST's (Figure 9). The solar radiation (Q_{SWR}) showed a marked increase from 87 W m^{-2} (15 September) to 240 W m^{-2} (17 September). Following this warming, horizontal advection caused mixed layer cooling during the period 20–22 September 2004. While 47% of upper-ocean cooling in AF was due to the horizontal advection, it was only 16% in FF suggesting that WCE had an impact on the SST cooling.

[36] In addition to both vertical mixing and horizontal divergence, vertical advection of cold water associated with the storm provided further cooling at 50 m. Consistent with FF, at 100 m depth, the rate of change of temperature was primarily due to vertical advection with a small contribution from horizontal advection. The important result here is that the horizontal advection is as large as the vertical diffusion term in the overall heat budget.

4.3. Experiment FA (Nonassimilation Initial Condition)

[37] An important shortcoming of the above experiments was the inconsistency in the location of the LC and WCE with observations. This deficiency was overcome in part by assimilating SSH on to the model. The heat-budget terms from FA were significantly different from the two other free-runs especially the amplitude of the warming and cooling (Figure 8). Except during Ivan's passing, all the terms showed a net warming tendency in the overall heat budget. Vertical mixing dominated the mixed layer cooling during Ivan's passage that accounted for 70% of the heat loss which was comparable with that in FF (74%). The contribution from surface heat flux resulted in a net warming, primarily due to the large reduction of latent heat flux ($\sim$18% from AF) associated with excessive SST cooling. Unlike the other two free-runs, in FA, there was an unexpected increase in the vertical-advection contribution (23%) to the total cooling. Since these experiments are forced with identical wind fields, differences in the upwelling driven by the curl of the wind stress are very unlikely. The physical processes leading to these differences are further discussed in the next section 5. Horizontal advection caused 16% of the cooling and the air-sea exchange accountable for the remainder (9% warming) during the storm. A comparison of balance terms between FA and FF suggests that the magnitude of the cooling actually increased dramatically in FA because of an increase in vertical advection (or upwelling) during the storm. Horizontal advection dominated the heat balance during 16–17 September 2004 following Ivan's passage. During this period, horizontal advection was responsible for 89% of upper-ocean warming and $\sim$14% came from the surface heat flux term. Both advection terms contributed to the net upper-ocean warming for several days after 18 September 2004.

[38] Beneath the mixed layer (at 50 and 100 m), temperature was changed primarily by vertical advection. At 50 m depth the sum of vertical (65%) and horizontal (22%) advective terms caused a net cooling and vertical diffusion accounted for the remainder. Wind-driven vertical mixing was still a significant contributor to the upper-ocean cooling at this depth. Upwelling was accountable for $\sim$92% of the

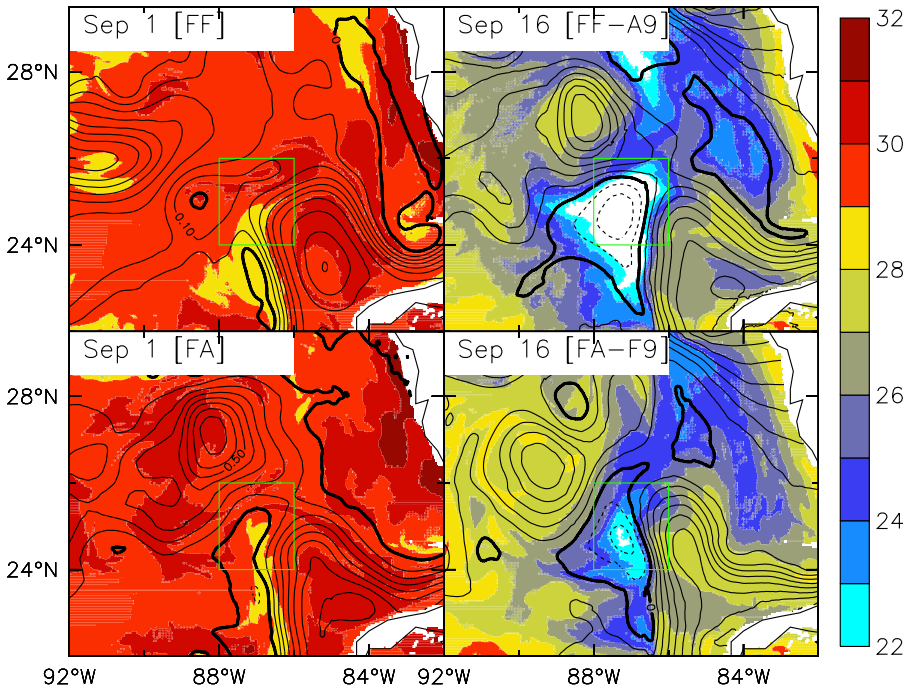

Figure 10. (left) Model SST (shaded, °C) and SSH (contours, m) on 1 September from FF and FA. (right) Same fields from FF-A9 and FA-F9. Contour interval for SST (SSH) is 1°C (0.1 m).

total −15558 W m^{-2} cooling at 100 m depth during the storm.

4.4. Experiments FA-F9 and FF-A9

[39] While the assimilation of SSH in FA improved the simulated location of LC and WCE, the inability to get the observed amplitude of SST cooling during the storm remained a major issue. FA-F9 and FF-A9 are designed (Table 1) to unravel this issue and to identify the scheme that most realistically simulates the storm-induced upper-ocean response. The initial (September 1) and final (September 16) SST (mixed layer temperature) and SSH from these runs are shown in Figure 10. The initial SST's (September 1) in FF and FA were >29°C almost everywhere in the GoM despite the marked differences in the location of the WCE. The cooling in FF-A9 due to Ivan's passage was in many ways identical to that in FA (strong cooling in the south and northeast of the WCE) though cooling of the latter area was less pronounced in FA (Figure 6). The area of extreme cooling in FA-F9 shifted farther south (north) with respect to FF (AF), analogous with the observations. The WCE drifted further southwestward from its initial position in the free-running model whereas the location of the WCE during the 16 day period was mostly unchanged in the assimilative run. Two conclusions can be drawn here (1) the storm-induced changes in the mixed layer were relatively insensitive to the prestorm conditions when assimilation was included and (2) free-run initialized with assimilation-model fields a few days prior to the storm reproduced the observed changes in the upper-ocean reasonably well.

[40] To quantify the physical processes leading to the differences in the mixed layer temperature we show heat-balance terms at 20 m depth from these experiments (Figure 8). A comparison of heat budget terms between FF-A9 and FA delineate the sensitivity of the model to initial conditions when assimilation is included. The adjustment of the model initial-state to the assimilative fields (SSH) was indicated by a sharp jump in balance terms during the first 7 days in FF-A9. The amplitude of the warming trend in FF-A9 before the passage of Ivan was much smaller than that in FA. Regardless of these differences, the physical processes leading to maximum cooling during Ivan's passage in both experiments (FA and FF-A9) were quite similar. The vertical diffusion contribution (mixed layer cooling) that increased by 4% in FF-A9 was balanced by the warming caused by surface heat flux (Q_S). Due to the differences in the location of WCE the rate of cooling in FA-F9 increased by 403 W m^{-2} from FF. These different cooling rates were caused primarily by differences in the horizontal advection which increased from 16% (−229 W m^{-2}, FF) to 35% (−629 W m^{-2}, FA-F9). The differences in the vertical mixing between the two runs accounted for 34 W m^{-2} cooling in FA-F9. Horizontal advective cooling was also found important in AF (Figure 8) during the storm period. The different cooling rates between AF (−2055 W m^{-2}) and FA-F9 (−1824 W m^{-2}) were caused in part by differences in horizontal advection owing to differences in the WCE location. Thus, depending upon the location of the WCE and LC region horizontal advection contributed between ∼16% and 47% to the total mixed-layer heat budget.

5. Discussions

[41] The impact of data assimilation on the storm-induced response during the passage of Hurricane Ivan (2–26 September 2004) is examined in a nested regional Gulf of Mexico (GoM) HYCOM model. This is achieved by two approaches: In the first approach (AF), we initialize the model with assimilation fields that include loop current

(LC) and warm core eddies (WCE) in the correct locations. In the second approach (FA), the assimilation is introduced during the model run time. Comparison of these two cases with a simulation that does not include data assimilation (FF) delineates the effects of data assimilation. The upper-ocean responses simulated by these three experiments (AF, FA and FF) were similar, but there were large differences in the location and amplitude of upper-ocean cooling. The differences in the location can be related to the differences in the simulated location of the WCE by these experiments. The different rate of SST cooling in these three experiments can be explained in part by differences in the prestorm thermal stratification. A shallower (deeper) thermocline together with a stronger (weaker) vertical temperature gradient is likely to produce stronger (weaker) upper-ocean cooling with a given surface wind force. The depth of the 20°C isotherm (D_{20}, measure of thermocline depth) prior to the passage of Ivan indicated a shallow thermocline west of ~87°W in all experiments (Figure 7). However, D_{20} in FA (~40 m) was much shallower than that in AF and FF (~80 m). Also noteworthy is the larger areal extent of this shallow zone in FA. The SSH in this region (west of LC) indicated the signature of a cyclonic eddy which appears to be generated by the shear instability associated with the LC (Figure 6). While a shallower D_{20} is expected because of this cyclonic eddy, the strength of the eddy simulated by AF and FF are weaker than FA. This results in a deeper D_{20} in AF and FF in comparison with FA.

[42] The enhanced SST cooling in those runs that included data assimilation were not a result of differences in vertical mixing or upwelling from the nonassimilative runs because under identical wind-forcing, they ought to be the same. A possible candidate for this enhanced SST cooling is the difference in the upper thermocline temperature gradient. To explore this further, we show in Figure 11 the time series of box average vertical temperature gradient in the upper 200 m from FF, FA, FF-A9 and FA-F9. Included also in Figure 11 is the mixed layer depth. Both model runs that included data assimilation (FA and FF-A9) indicated a thin prestorm mixed layer and a sharp upper thermocline temperature gradient which in turn enhanced the upper-ocean cooling via vertical mixing and upwelling. On the other hand, a weak vertical temperature gradient and somewhat thicker mixed layer during the prestorm period in FF and FA-F9 limited the cooling. Vertical sections of temperature (September 16), vertical diffusion coefficient (K_T, $m^2\ s^{-1}$, September 15) and vertical velocity (10^{-4} m s^{-1}, September 15) along 24°N are depicted in Figure 11. The location of maximum vertical mixing occurred to the right of Ivan's path as expected because the area of strongest wind speeds in a moving hurricane is in the northeast quadrant. The deep thermocline (and high heat storage) associated with the LC east of the track greatly limited the availability of cold water to the surface from below. In contrast, the coldest surface water was located somewhat to the left of Ivan's track.

[43] The coincidence of the maximum cooling with the shallowest thermocline depth (20°C isotherm depth was located at ~75 m or less) in all experiments during Ivan's passage suggests that both upwelling and vertical mixing contributed to the upper-ocean cooling. It should be noted that the shallow thermocline (88°–86°W) in Figure 11 (after Ivan) below ~100 m were not greatly different from those before the storm. If upwelling occurs simultaneously with vertical mixing, then the mixed layer becomes shallower which in turn enhances surface cooling. The vertical velocity of the assimilative runs (FA and FF-A9) predicted slightly higher values ($\sim 15 \times 10^{-4}$ m s^{-1}) than the free-runs ($\sim 10 \times 10^{-4}$ m s^{-1}). The center of the upwelling was closer to the center of the storm and there was no bias to the right of the storm track. A further increase in surface cooling is possible if the upper thermocline temperature gradient is large. The different vertical-mixing cooling rates between FF (−1045 W m^{-2}) and FA (−2002 W m^{-2}) were caused primarily by differences in the initial thermal stratification (Figure 11) and could not be explained by the differences in the vertical diffusion coefficients. For example, the volume average values of K_T (88°–86°W, 24°–26°N, 0–50 m) from FF and FA on September 15 was 0.044 and 0.028 $m^2\ s^{-1}$, respectively, which did not support a greater mixing across the mixed layer base in FA. Thus, it is evident that the shallower thermocline along with stronger upwelling and a larger vertical temperature gradient in the assimilation runs (FA and FF-A9) resulted in much stronger upper-ocean cooling than the runs that do not include data assimilation (AF, FF and FA-F9).

[44] Although the model results presented here captured the basic details of the processes leading to the upper-ocean cooling response to Ivan, there are several model-data discrepancies that need to be addressed. The experiments reported here (nonassimilative runs) dramatically illustrate the sensitivity of the timing of eddy-shedding behavior to changes in the initial conditions. This issue will be explored fully in the near future through a series of model sensitivity experiments. Though surface heat fluxes are found insignificant in the mixed-layer heat budget, considerable uncertainty remains in the transfer coefficients that need further investigation. The results presented here are likely sensitive to the choice of vertical mixing scheme (GISS) employed here. However, the overall rate of cooling and mixed-layer deepening would remain qualitatively similar. Finally, a shallower thermocline and an associated excessive SST cooling in the assimilative runs remain a concern. This deficiency of the model may be associated with the *Cooper and Haines*'s [1996] downward projection technique that was used here; this issue will be addressed in the near future.

6. Summary

[45] A 20 layer in the vertical and 1/25° (~4 km) horizontal resolution HYCOM Gulf of Mexico (GoM) model was employed to investigate the three-dimensional oceanic processes responding to Hurricane Ivan which traversed the GoM during the period 14–16 September 2004. By conducting several model experiments, we examined the sensitivity of the location of the WCE and the LC to the initial conditions and compared a nonassimilative simulation with one that included assimilation of SSH. The storm induced changes were insensitive to the initial conditions in the assimilative runs but highly sensitive in the nonassimilation owing to variations in the trajectories of the WCE. SST decreased ~6°C as Ivan passed over the GoM at

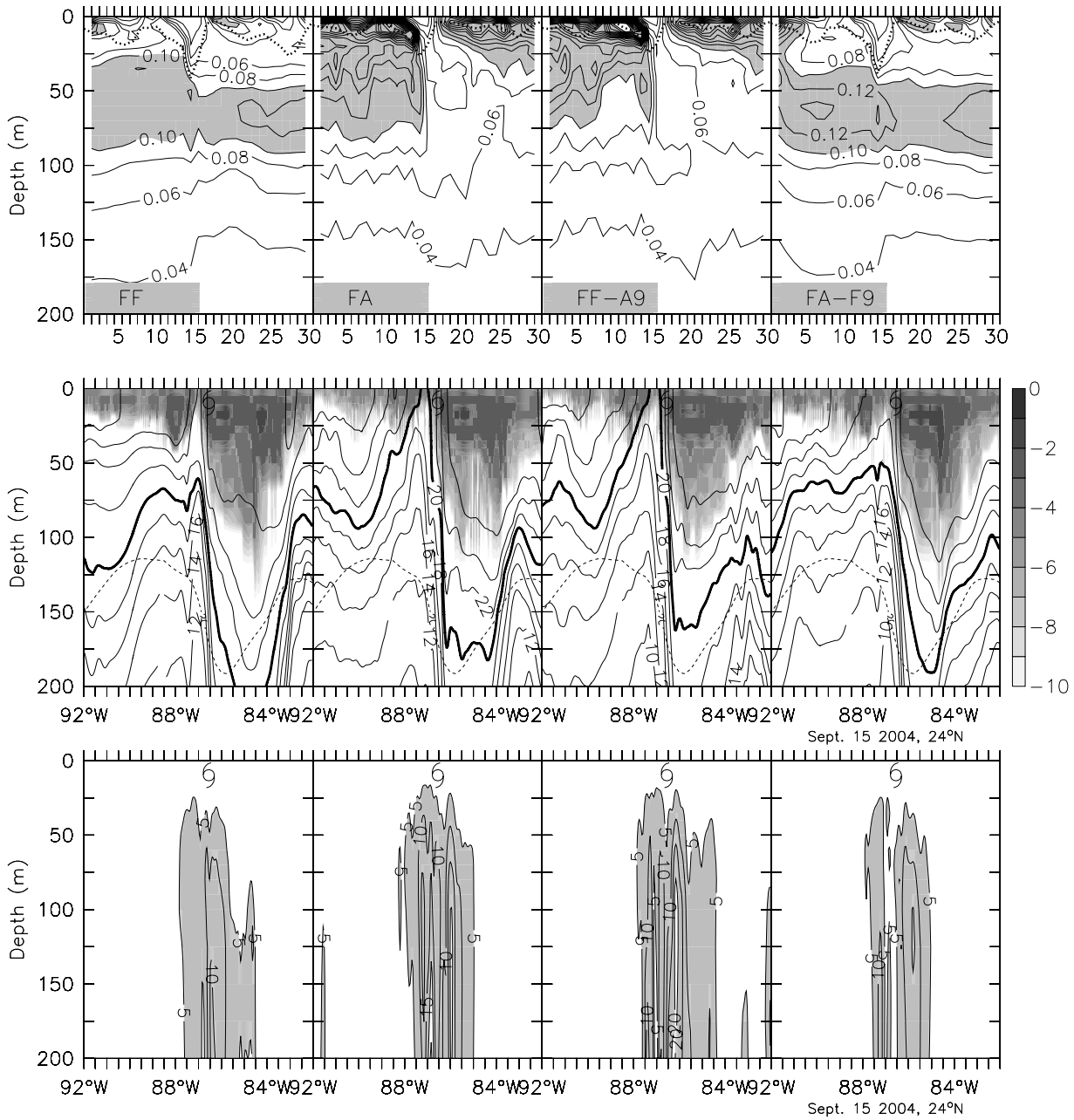

Figure 11. (top) Time series of vertical temperature gradient (°C m^{-1}, contours) and mixed-layer depth (m, dotted line) averaged over 88°–86°W, 24°–26°N. (middle) Meridional vertical sections (24°N) of temperature (contours) on 16 September (dashed line indicates the climatological September mean position of the depth of 20°C isotherm from the General Digital Environmental Model (GDEM), and shaded regions indicate vertical diffusion coefficient (ln[K_T], natural logarithm of K_T in m^2 s^{-1})). (bottom) Vertical velocity (>5 × 10^{-4} m s^{-1}) from FF, FA, FF-A9 and FA-F9 on 15 September 2004. Longitudinal position of Ivan's eye at 24°N is marked.

6.5 m s^{-1} in agreement with the TMI observations. The location of maximum cooling associated with Ivan's passage varied depending upon the location of the WCE. However, maximum cooling in all experiments occurred at the center of the storm track (south of ~26°N); this differs from several observations and modeling studies where cold water areas were found to the right of the storm track. While the maximum vertical mixing was experienced in the northeast quadrant of the storm, the lack of corresponding SST response was due to the underlying thermal structure of the water column. Inclusion of data assimilation did not greatly alter the pattern of SST cooling, but caused pronounced SST cooling (>8°C) over a larger area. In the WCE region the SST cooling was only 1°–2°C.

[46] The physical processes underlying the upper-ocean cooling that occurred during the hurricane passage were

quantified. Overall, ~64% of the cooling was due to vertical mixing caused by the turbulence generated from the strong shear-stress across the base of the mixed layer. However, this value varied from 58.8% (all nonassimilative runs) to 71.8% (all assimilative runs) depending on the model experiments. In all experiments, the vertical diffusion term contributed to the mixed-layer heat budget only during 13–17 September. The dominant role of entrainment mixing was also previously noted by *Jacob et al.* [2000] based on observations and by *Price* [1981] based on model results. Vertical advection (upwelling) caused a significant portion of cooling (23.4%) in those runs that included data assimilation; a three fold increase from the free runs average (7%). This enhanced upper-ocean cooling was caused primarily by the initial thermal stratification; a shallower thermocline (Figure 7) and a stronger upper-thermocline gradient (Figure 11). In all experiments the air-sea exchange was a small component of the mixed layer heat budget which overall accounted for ~4% and in some cases actually contributed to net surface warming. The mixed-layer heat balance following the passage of Ivan was dominated by horizontal advection due to oscillations in velocity components which are associated with inertia-gravity waves induced by the storm. Vertical velocities with alternating upward and downward oscillations associated with the inertial-gravity waves also persisted in the wake of the storm. Overall the rate of cooling below the mixed layer (50 m) was largely due to vertical divergence (~54%); the combined effects of horizontal advection (~26%) and vertical mixing (~20%) accounted for the remainder. The storm induced vertical motion led to large vertical advection at 100 m which was responsible for ~90% of the rate of heat change.

[47] **Acknowledgments.** This paper is a contribution to the coastal ocean nesting studies project sponsored by the Office of Naval Research (ONR) under program element 601153N. It is also a contribution to the NRL project Slope to Shelf Energetics and Exchange Dynamics (SEED) also under program element 601153N. The simulations were performed on IBM-SP4 workstations at the Naval Oceanographic Office under a grant of computer time from the DoD High Performance Computer Modernization Office (HPCMO). Alan Wallcraft is recognized for substantial contribution to this effort through his work on model development and his computer expertise. The authors wish to thank Ole Martin Smedstad (NRL/PSI) for helping us with the assimilation run and Sang-ki Lee (RSMAS/CIMAS) for sharing heat-budget codes. The altimeter products were produced by Ssalto/Ducacs and distributed by Aviso, with support from Cnes. SSH data are provided by Robert R. Leben, CCAR, Colorado. TMI data are produced by Remote Sensing Systems and sponsored by the NASA Earth Science project. Comments by the two anonymous reviewers improved the quality of the manuscript.

References

Bleck, R., G. R. Halliwell, A. J. Wallcraft, S. Carroll, K. Kelly, K. Rushing, (2002), Hybrid Coordinate Ocean Model (HYCOM) user's manual: Details of the numerical code, Univ. of Miami, Miami, Fla. (Available at http://hycom.rsmas.miami.edu)

Brooks, D. A. (1983), The wake of Hurricane Allen in the western Gulf of Mexico, *J. Phys. Oceanogr.*, *13*, 117–129.

Browning, G. L., and H.-O. Kreiss (1982), Initialization of the shallow water equations with open boundaries by the bounded derivative method, *Tellus*, *34*, 334–351.

Browning, G. L., and H.-O. Kreiss (1986), Scaling and computation of smooth atmospheric motions, *Tellus, Ser. A*, *38*, 295–313.

Buck, A. L. (1981), New equations for computing vapor pressure and enhancement factor, *J. Appl. Meteorol.*, *20*, 1527–1532.

Canuto, V. M., A. Howard, Y. Cheng, and M. S. Dubovikov (2001), Ocean turbulence. part I: One-point closure model: Momentum and heat vertical diffusivities, *J. Phys. Oceanogr.*, *31*, 1413–1426.

Canuto, V. M., A. Howard, Y. Cheng, and M. S. Dubovikov (2002), Ocean turbulence. part II: Vertical diffusivities of momentum, heat, salt, mass and passive scalars, *J. Phys. Oceanogr.*, *32*, 240–264.

Canuto, V. M., A. Howard, P. J. Hogan, Y. Cheng, M. S. Dubovikov, and L. M. Montenegro (2004), Modeling ocean deep convection, *Ocean Modell.*, *7*, 75–95.

Chassignet, E. P., H. E. Hurlburt, O. M. Smedstad, G. R. Halliwell, P. J. Hogan, A. J. Wallcraft, R. Baraille, and R. Bleck (2007), The HYCOM (Hybrid Coordinate Ocean Model) data assimilative system, *J. Mar. Syst.*, *65*, 60–83.

Cooper, M., and K. Haines (1996), Data assimilation with water property conservations, *J. Geophys. Res.*, *101*, 1059–1077.

Dickey, T., et al. (1998), Upper-ocean temperature response to Hurricane Felix as measured by the Bermuda Test-bed Mooring, *Mon. Weather Rev.*, *126*, 1195–1200.

Elliott, B. A. (1982), Anticyclonic rings in the Gulf of Mexico, *J. Phys. Oceanogr.*, *12*, 1292–1309.

Goni, G. J., and J. A. Trinanes (2003), Ocean thermal structure monitoring could air in the intensity forecast of tropical cyclones, *Eos Trans. AGU*, *84*(51), 573, 577–578.

Greatbatch, R. J. (1985), On the role played by upwelling of water in lowering sea surface temperatures during the passage of a storm, *J. Geophys. Res.*, *90*, 11,751–11,755.

Halliwell, G. R. (2004), Evaluation of vertical coordinate and vertical mixing algorithms in the Hybrid-Coordinate Ocean Model (HYCOM), *Ocean Modell.*, *7*, 285–322.

Hong, X., S. W. Chang, S. Raman, L. K. Shay, and R. Hodur (2000), The interaction between Hurricane Opal (1995) and a warm core ring in the Gulf of Mexico, *Mon. Weather Rev.*, *128*, 1347–1365.

Jacob, S. D., and L. K. Shay (2003), The role of oceanic mesoscale features on the tropical cyclone-induced mixed layer response: A model study, *J. Phys. Oceanogr.*, *33*, 649–676.

Jacob, S. D., L. K. Shay, and A. J. Mariano (2000), The 3D oceanic mixed layer response to Hurricane Gilbert, *J. Phys. Oceanogr.*, *30*, 1407–1429.

Kara, A. B., P. A. Rochford, and H. E. Hurlburt (2002), Air-sea flux estimates and the 1997–1998 ENSO event, *Boundary Layer Meteorol.*, *103*, 439–458.

Large, W. G., J. C. McWilliams, and S. C. Doney (1994), Oceanic vertical mixing: Review and a model with a non-local boundary layer parameterization, *Rev. Geophys.*, *32*, 363–403.

Large, W. G., G. Danabasoglu, S. C. Doney, and J. C. McWilliams (1997), Sensitivity to surface forcing and boundary layer mixing in a global ocean model: Annual mean climatology, *J. Phys. Oceanogr.*, *27*, 2418–2447.

Leipper, D. F. (1967), Observed ocean conditions and Hurricane Hilda, 1964, *J. Atmos. Sci.*, *24*, 182–196.

Leipper, D. F., and D. Volgenau (1972), Hurricane heat potential of the Gulf of Mexico, *J. Phys. Oceanogr.*, *2*, 218–224.

Louis, J. F. (1979), A parametric model of vertical eddy fluxes in the atmosphere, *Boundary Layer Meteorol.*, *17*, 187–202.

Martin, P. J. (1985), Simulation of the mixed layer at OWS November and Papa with several models, *J. Geophys. Res.*, *90*, 903–916.

Mellor, G. L., and T. Yamada (1982), Development of a turbulence closure model for geophysical fluid problems, *Rev. Geophys.*, *20*, 851–875.

Powell, M. D., P. J. Vickery, and T. A. Reinhold (2003), Reduced drag coefficient for high wind speeds in tropical cyclones, *Nature*, *422*, 279–283.

Price, J. F. (1981), Upper ocean response to a hurricane, *J. Phys. Oceanogr.*, *11*, 153–175.

Price, J. F., R. A. Weller, and R. Pinkel (1986), Diurnal cycling: Observations and models of the upper-ocean response to diurnal heating, cooling, and wind mixing, *J. Geophys. Res.*, *91*, 8411–8427.

Price, J. F., T. B. Sanford, and G. Z. Forristall (1994), Forced stage response to a moving hurricane, *J. Phys. Oceanogr.*, *24*, 233–260.

Sanford, T. B., P. G. Black, J. R. Haustein, J. W. Feeney, G. Z. Forristall, and J. F. Price (1987), Ocean response to a hurricane. part I: Observations, *J. Phys. Oceanogr.*, *17*, 2065–2083.

Scharroo, R., W. H. F. Smith, and J. L. Lillibridge (2005), Satellite altimetry and the intensification of Hurricane Katrina, *Eos Trans. AGU*, *86*(40), 366.

Shay, L. K., and R. L. Elsberry (1987), Near-inertial ocean current response to Hurricane Frederic, *J. Phys. Oceanogr.*, *17*, 1249–1269.

Shay, L. K., R. L. Elsberry, and P. G. Black (1989), Vertical structure of the ocean current response to a hurricane, *J. Phys. Oceanogr.*, *19*, 649–669.

Shay, L. K., A. J. Mariano, S. D. Jacob, and E. H. Ryan (1998), Mean and near-inertial ocean current response to Hurricane Gilbert, *J. Phys. Oceanogr.*, *28*, 858–889.

Shay, L. K., G. J. Goni, and P. G. Black (2000), Effects of warm oceanic feature on Hurricane Opal, *Mon. Weather Rev.*, *128*, 1366–1383.

Vukovich, F. M., and E. Crissman (1986), Aspects of warm rings in the Gulf of Mexico, *J. Geophys. Res.*, *91*, 2645–2660.

Wang, D. W., D. A. Mitchell, W. J. Teague, E. Jarosz, and M. S. Hulbert (2005), Extreme waves under Hurricane Ivan, *Science*, *309*, 896, doi:10.1126/science.1112509.

Whitaker, W. D. (1967), Quantitative determination of heat transfer from sea to air during passage of Hurricane Betsy, M. S. thesis, Texas A&M Univ., College Station.

P. J. Hogan and T. G. Prasad, Naval Research Laboratory, Code 7323, Stennis Space Center, MS 39529, USA. (thoppil@nrlssc.navy.mil)